


 Cite this: *RSC Adv.*, 2023, 13, 1412

# Magnetically separable triazine-based Cu(II)–vitamin B<sub>5</sub> complex in nitromethane toward efficient heterogeneous cyanation reaction of aryl halides†

 Farzaneh Karimi,‡ Masoumeh Jadidi Nejad,  ‡ Arefe Salamatmanesh and Akbar Heydari\*

In the current study, a highly efficient heterogeneous copper catalyst has been developed by supporting copper acetate on a magnetically separable triazine–vitamin B<sub>5</sub> system. After the successful characterization of the prepared nanoparticles by various techniques such as FT-IR, FE-SEM, EDX/MAP, XRD, TEM, TGA, VSM, and ICP-OES, the catalytic efficiency of them were evaluated in the cyanation reaction of aryl halides in the presence of nitromethane as a non-toxic and cost-effective cyanation source. The cyanation products were obtained in desirable yields. Notably, the magnetic nanocatalyst can be easily recovered and reused at least five times without a significant decrease in its performance.

 Received 27th September 2022  
 Accepted 20th December 2022

DOI: 10.1039/d2ra06104j

[rsc.li/rsc-advances](https://rsc.li/rsc-advances)

## 1 Introduction

Aromatic nitriles are an important class of versatile scaffolds present in natural compounds and many synthetic organic products, such as dyes, pharmaceuticals, agrochemicals, and herbicides.<sup>1</sup> They can also be transformed into a variety of organic compounds such as imines, aldehydes, amines, amides, esters, carboxylic acids, and tetrazoles.<sup>2</sup> In recent decades, novel methodologies have been developed for the introduction of a nitrile functional group into an aromatic framework. The diazotization of anilines followed by the Sandmeyer reaction<sup>3</sup> and also the Rosenmund–von Braun reaction<sup>4</sup> have been known as classic synthetic methods toward aryl nitriles. Since then, a series of transition metal-catalyzed protocols have been reported for the cyanation reactions by using diverse cyano sources such as KCN,<sup>5</sup> NaCN,<sup>6</sup> Zn(CN)<sub>2</sub>,<sup>7</sup> CuCN,<sup>8</sup> and TMSCN.<sup>9</sup> Nevertheless, most of them are confronted with significant drawbacks including the use of toxic metal cyanides in stoichiometric amounts and the requirement of harsh reaction conditions. To overcome this problems, several less-toxic metal-free cyanide sources including malononitrile,<sup>10</sup> butyronitrile,<sup>11</sup> acetonitrile,<sup>12</sup> benzyl cyanide,<sup>13</sup> AIBN,<sup>14</sup> *etc.* have been disclosed. Furthermore, some other organic compounds, which can generate cyano groups *in situ* have been employed as indirect cyanation

sources. Explored examples of such cyanation reagents include NH<sub>4</sub>I/DMF,<sup>15</sup> NH<sub>4</sub>HCO<sub>3</sub>/DMSO,<sup>16</sup> NH<sub>4</sub>HCO<sub>3</sub>/DMF,<sup>17</sup> *t*-BuNC,<sup>18</sup> *etc.* Recently, nitromethane has also been introduced as a potentially valuable indirect organic cyano source for the cyanation of organic scaffolds, because of its chemical stability, and low-cost commercial availability. Nevertheless, there are very few reports on the use of nitromethane as a cyanation reagent in the field of metal-catalyzed aromatic CCN bond formation. So, it is still demanding to make attempts in this direction.<sup>19</sup>

Over the recent past decades, various transition metals, such as Pd,<sup>20</sup> Co,<sup>21</sup> Ni,<sup>22</sup> Cu,<sup>10</sup> Rh<sup>23</sup> and Zn<sup>24</sup> have been utilized to catalyze cyanation reactions of aryls and aryl halides using different cyanation sources. Among them, the use of Cu as a readily available and inexpensive transition metal can be desirable.<sup>17,19</sup> However, most of these reported metal-catalyzed cyanation reactions have adopted a homogeneous approach, which suffer from serious limitations including high expenses, problematic separation (in some cases non-separable), and non-reusability of metal catalysts. To meet these restrictions as well as minimize possible pollution caused by toxic metal discharge in some homogeneous protocols, a wide range of heterogeneous metal-incorporating catalytic systems have been developed for cyanation transformations.<sup>25</sup> Magnetic nanoparticles have been well known as one of the most promising heterogeneous nanostructures, which have unique physico-chemical features in addition to being easily recoverable and reusable.<sup>26</sup>

Until now, various reports have been presented about the use of ligands in the cyanation reaction, and by examining the used ligands and the importance of ligands containing nitrogen

Chemistry Department, Tarbiat Modares University, P.O. Box 14155-4838, Tehran, Iran. E-mail: heydar\_a@modares.ac.ir; Fax: +98-21-82883455; Tel: +98-21-82883444

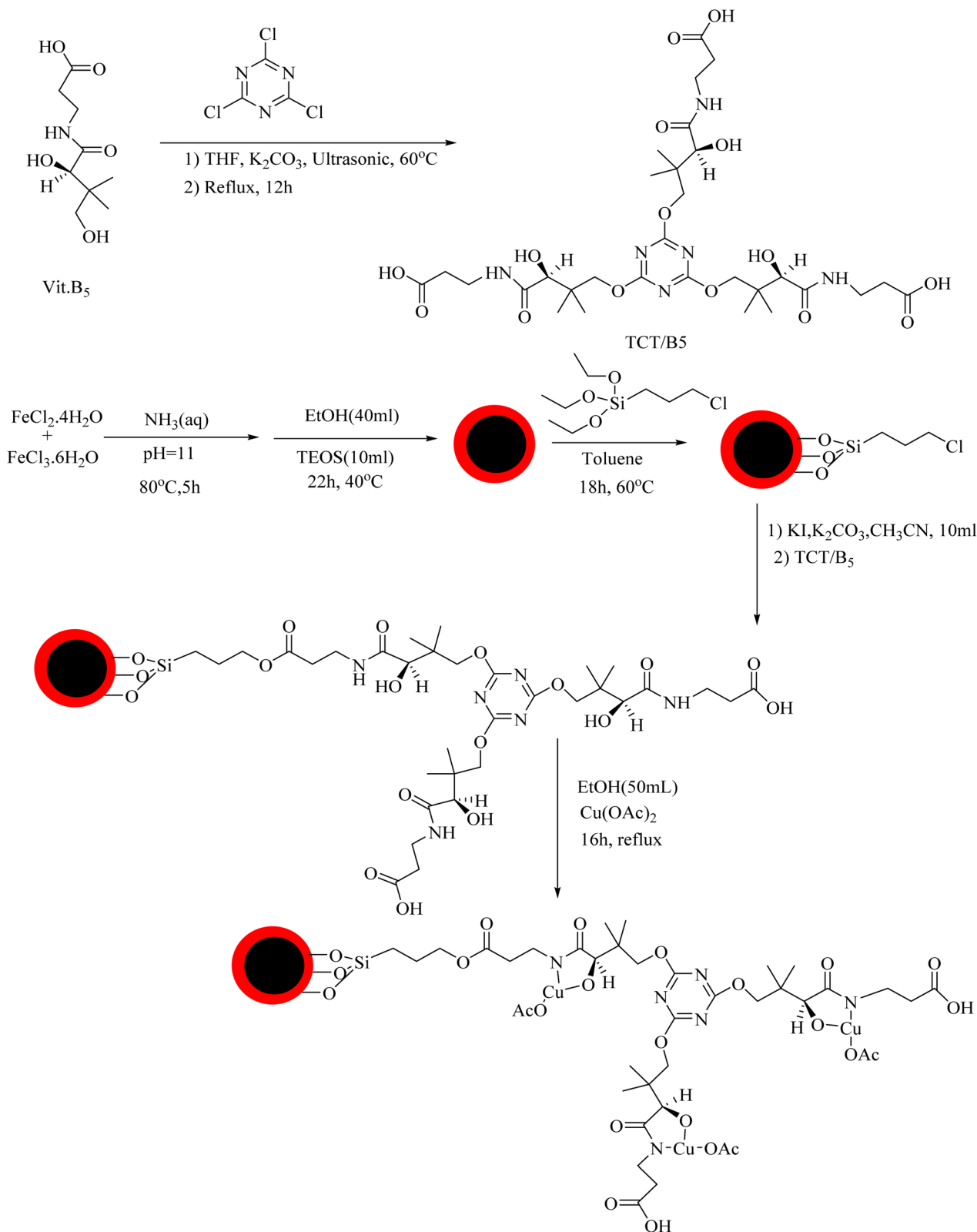
† Electronic supplementary information (ESI) available. See DOI: <https://doi.org/10.1039/d2ra06104j>

‡ These authors contributed equally.



and oxygen in binding to various metals and forming stable complexes,<sup>27–30,19a</sup> we chose vitamin B<sub>5</sub> as a suitable ligand for this reaction.

To the best of our knowledge, no heterogeneous copper catalyst has been reported for the cyanation of aryl halides using nitromethane as an indirect organic nitrile source. In this work,



Scheme 1 Preparation of Fe<sub>3</sub>O<sub>4</sub>@SiO<sub>2</sub>-TCT/B<sub>5</sub>-Cu(II).



we designed and synthesized a novel heterogeneous copper-incorporating nanocatalyst by loading copper acetate on a magnetically recyclable triazine–vitamin B<sub>5</sub> system for the synthesis of aryl nitriles from aryl halide substrates in presence of nitromethane.

## 2 Experimental

### 2.1. General remarks

All required materials were purchased from Aldrich and Merck companies and were used without any further purification. The reaction was monitored by thin-layer chromatography. TLC was performed on glass plates incorporated with silica-gel 60 F-254. Infrared spectrums (IR) were determined by grade KBr on a Nicolet FT-IR 100 spectrometer. X-ray diffraction (XRD) data were obtained at room temperature by a Philips X-pert 1710. The size and morphology of the nanoparticles were determined by scanning electron microscopy (SEM) using a TESCAN MIRA III FE-SEM. Also, the elemental composition of the nanoparticles was studied by energy-dispersive X-ray (EDAX). Transmission electron microscopy (TEM) was performed using a Philips CM 120 at 120 kV. Thermal gravimetric analysis (TGA) was performed by a thermal analyzer with a heating rate of 10 °C min<sup>-1</sup> in the range of 25–800 °C under the following air.

### 2.2. Synthesis of TCT/B<sub>5</sub>

Cyanuric chloride (1 mmol or 0.18 g) was dissolved in 5 mL of anhydrous tetrahydrofuran (THF). The resulting solution was then slowly added to a solution of vitamin B<sub>5</sub> in anhydrous THF (5 mL) and ultrasonicated at 60 °C. Potassium carbonate (1 mmol or 0.138 g) was added to the reaction mixture, and the solution was kept under the same conditions for 3 h and then stirred for 12 h at 70 °C. Finally, the reaction mixture was centrifuged, and the product was separated, washed with anhydrous THF, and dried in a vacuum oven at 70 °C.

### 2.3. Synthesis of Fe<sub>3</sub>O<sub>4</sub>@SiO<sub>2</sub>

A mixture of FeCl<sub>3</sub>·6H<sub>2</sub>O (5 mmol or 1.35 g) and FeCl<sub>2</sub>·4H<sub>2</sub>O (2.5 mmol or 0.5 g) in 50 mL deionized water was ultrasonicated for 10 min to be completely dispersed. While the solution was being stirred at room temperature, 20 mL of ammonia solution (37%) was added dropwise until reaching pH = 11. The solution was then stirred under a nitrogen atmosphere at 80 °C for 5 h. Thereafter, the solution was cooled down to 40 °C, 40 mL of ethanol was added, and the reaction mixture was stirred for 30 min. Tetraethyl orthosilicate (10 mL) was gradually added to the reaction mixture and it was then placed under a nitrogen atmosphere at 40 °C for 22 h. The Fe<sub>3</sub>O<sub>4</sub>@SiO<sub>2</sub> product was separated by applying an external magnetic field, washed several times with water and ethanol, and dried in a vacuum oven at 80 °C.

### 2.4. Synthesis of Fe<sub>3</sub>O<sub>4</sub>@SiO<sub>2</sub>-TCT/B<sub>5</sub>

Anhydrous toluene (50 mL) was added to 0.2 g Fe<sub>3</sub>O<sub>4</sub>@SiO<sub>2</sub>, and the solution was ultrasonicated for 15 min to be completely dispersed. Then, (3-chloropropyl)trimethoxysilane (10 mL) was

added to the dispersion, and the mixture was stirred at 60 °C for 18 h under a nitrogen atmosphere. The nanoparticles were separated by applying an external magnetic field, washed several times with anhydrous toluene, and dried in a vacuum oven at 80 °C. First, potassium iodide (2 mmol or 0.332 g), then potassium carbonate (2 mmol or 0.276 g), and, finally, TA/B<sub>5</sub> (0.2 g) were added to Fe<sub>3</sub>O<sub>4</sub>@SiO<sub>2</sub>-Cl (0.2 g) dispersed in 10 mL acetonitrile, and the mixture was refluxed for 12 h. The nanoparticles were then separated by applying an external magnetic field, washed several times with water and ethanol, and dried in a vacuum oven at 80 °C.

### 2.5. Synthesis of Fe<sub>3</sub>O<sub>4</sub>@SiO<sub>2</sub>-TCT/B<sub>5</sub>-Cu(II)

Fe<sub>3</sub>O<sub>4</sub>@SiO<sub>2</sub>-TCT/B<sub>5</sub> (0.2 g) was dispersed in 50 mL ethanol through 15 min ultrasonication. Next, 1 mmol of copper(II) acetate monohydrate dissolved in ethanol was added dropwise to the dispersion. The resulting mixture was then refluxed for 16 h. The nanoparticles are separated by applying an external electric field, washed several times with ethanol, and dried in a vacuum oven at 60 °C.

### 2.6. Procedure route for the synthesis of aryl cyanides

First, 4-iodoanisole (1 mmol or 0.234 g), nitromethane (3 mmol or 0.183 g), potassium carbonate (1 mmol or 0.138 g), and the catalyst (30 mg) were weighed and poured into a glass tube. Then, 3 mL dimethyl sulfoxide (solvent) was added and the mixture was stirred at 100 °C for 12 h. Thin-layer chromatography was used to monitor the progress of the reaction. Upon the completion of the reaction, the reaction mixture was cooled down to room temperature, and the catalyst was removed by a magnet. The reaction mixture was then extracted by water and ethyl acetate. After any remaining water droplets were removed from the organic phase by using anhydrous sodium sulfate, the solvent was evaporated under a vacuum. Finally, the purification process was carried out using silica gel plates and ethyl acetate : hexane (1 : 9) solvent.

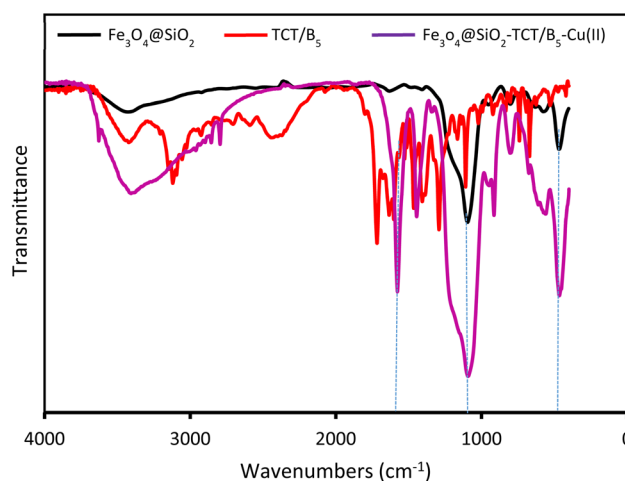


Fig. 1 The FT-IR spectra of Fe<sub>3</sub>O<sub>4</sub>@SiO<sub>2</sub> (black curve), TCT/B<sub>5</sub> (red curve), and Fe<sub>3</sub>O<sub>4</sub>@SiO<sub>2</sub>-TCT/B<sub>5</sub>-Cu(II) (violet curve).



## 3 Results and discussion

### 3.1. Catalyst preparation

The preparation process of the proposed  $\text{Fe}_3\text{O}_4@\text{SiO}_2\text{-TCT/B}_5\text{-Cu(II)}$  nanocatalyst is illustrated in Scheme 1 as explained in the experimental section. Then to elucidate the structure of the prepared nanocatalyst, several analyses including FT-IR, XRD, SEM, TEM, EDX, TGA, and ICP were carried out.

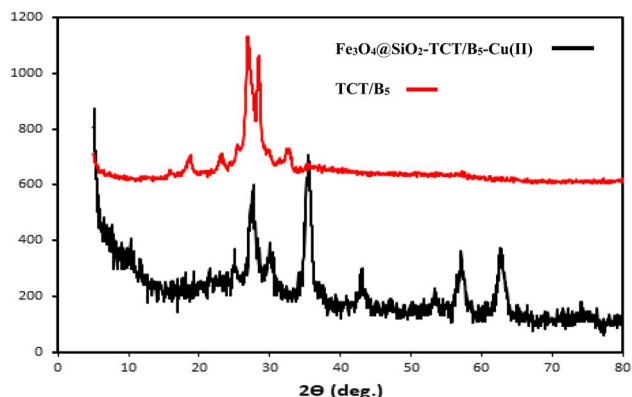


Fig. 2 XRD patterns of TCT/B<sub>5</sub> (red curve) and  $\text{Fe}_3\text{O}_4@\text{SiO}_2\text{-TCT/B}_5\text{-Cu(II)}$  (black curve).

### 3.2. Catalyst characterization

**3.2.1. FT-IR.** FT-IR spectra of  $\text{Fe}_3\text{O}_4@\text{SiO}_2$ , TCT/B<sub>5</sub>, and  $\text{Fe}_3\text{O}_4@\text{SiO}_2\text{-TCT/B}_5\text{-Cu(II)}$  are shown in Fig. 1. In the spectrum of  $\text{Fe}_3\text{O}_4@\text{SiO}_2$ , the stretching and bending vibrations of the O–H bond are observed at around  $3429\text{ cm}^{-1}$  and  $1632\text{ cm}^{-1}$ , respectively. Also, peaks appearing at  $1095\text{ cm}^{-1}$  and  $466\text{ cm}^{-1}$  are associated with the stretching and bending vibrational modes of Si–O–Si, respectively. In addition, the characteristic peak that appeared at  $574\text{ cm}^{-1}$  can be related to the Fe–O stretching. In the FT-IR spectrum of TCT/B<sub>5</sub>, the bands located at  $1717\text{ cm}^{-1}$ ,  $1634\text{ cm}^{-1}$  and  $1602\text{ cm}^{-1}$  can be assigned to ester, acid and amid carbonyl groups, respectively. The appearance of a characteristic peak at  $1717\text{ cm}^{-1}$  can be ascribed to ester, indicating the formation of the covalent bond between TCT and vitamin B<sub>5</sub>. There are two absorption bands in the area of  $1400\text{--}1460\text{ cm}^{-1}$  and  $1100\text{--}1290\text{ cm}^{-1}$ , which are associated with the stretching vibrations of the C–N bond and C–O bond, respectively. Also, peaks observed at around  $3422\text{ cm}^{-1}$  and  $2925\text{ cm}^{-1}$  are allocated to O–H and C–H aliphatic stretching vibrations, respectively. The characteristic peaks in the FT-IR spectrum of  $\text{Fe}_3\text{O}_4@\text{SiO}_2\text{-TCT/B}_5\text{-Cu(II)}$  are mainly observed at  $3406\text{ cm}^{-1}$ ,  $1577\text{ cm}^{-1}$ ,  $1440\text{ cm}^{-1}$ ,  $1092\text{ cm}^{-1}$ , and  $465\text{ cm}^{-1}$ , which can be respectively related to the stretching vibrations of O–H, C=N triazine ring, C–N, Si–O–Si and Fe–O bonds, indicating the successful attachment of

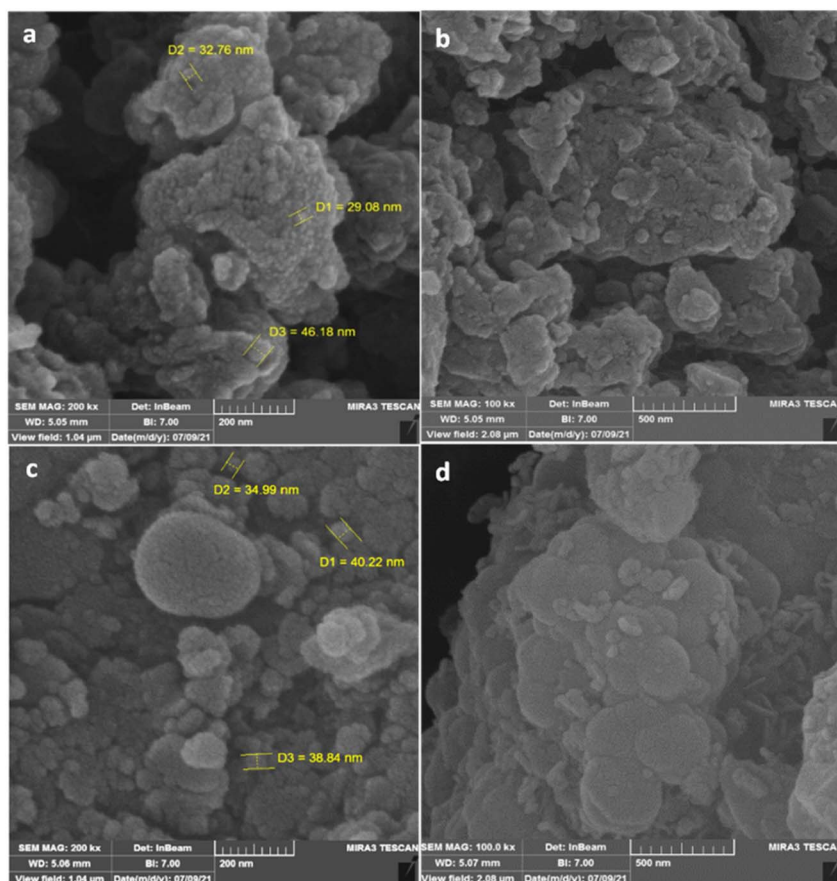


Fig. 3 The SEM images of TCT/B<sub>5</sub> (a and b) and  $\text{Fe}_3\text{O}_4@\text{SiO}_2\text{-TCT/B}_5\text{-Cu(II)}$  (c and d).



TCT/B<sub>5</sub> to the support. In addition, due to the coordination of some ligand groups with Cu(II) species, the intensity of some TCT/B<sub>5</sub> peaks in the final catalyst has decreased.

**3.2.2. XRD.** XRD results of TCT/B<sub>5</sub> and Fe<sub>3</sub>O<sub>4</sub>@SiO<sub>2</sub>-TCT/B<sub>5</sub>-Cu(II) were depicted in Fig. 2. As shown in the XRD pattern of TCT/B<sub>5</sub>, there are peaks to those of ligand structure in the final catalyst XRD pattern. As illustrated in the XRD pattern of Fe<sub>3</sub>O<sub>4</sub>@SiO<sub>2</sub>-TCT/B<sub>5</sub>-Cu(II), the diffraction peaks at  $2\theta$  values of 30.74°, 35.89°, 43.44°, 53.94°, 57.64° and 63.24° correspond to (220), (311), (400), (422), (422), (511) and (440) planes of Fe<sub>3</sub>O<sub>4</sub>, which can be readily indexed to the standard spinel cubic magnetite (JCPDS no. 19-0629). Also, the broad peak at  $2\theta = 20$  to 30 can be assigned to the amorphous SiO<sub>2</sub> phase. The diffraction peaks at  $2\theta$  values of 29.54° and 32.19° can be attributed to ligand structure in the final catalyst. As shown in the XRD pattern of TCT/B<sub>5</sub>, there are peaks similar to those of ligand structure in the final catalyst XRD pattern, confirming the success of ligand binding to the magnetic support.

**3.2.3. SEM.** The morphology and size of nanocatalysts were investigated by FE-SEM analysis. The SEM images of TCT/B<sub>5</sub> and Fe<sub>3</sub>O<sub>4</sub>@SiO<sub>2</sub>-TCT/B<sub>5</sub>-Cu(II) were depicted in Fig. 3a-d. As it

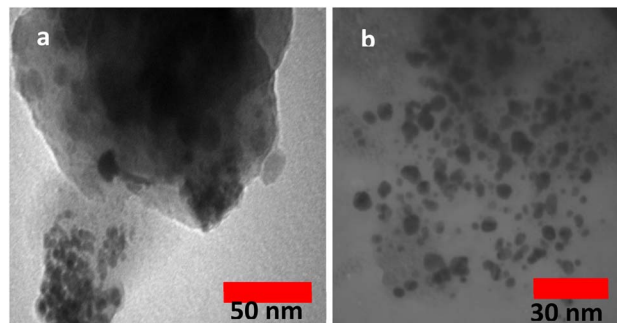
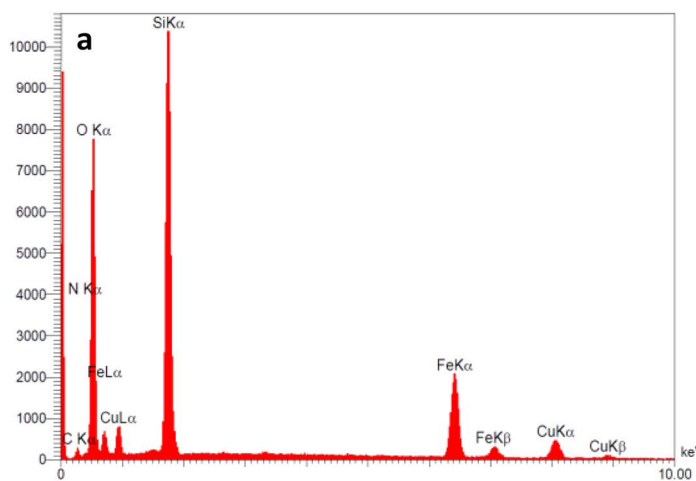


Fig. 5 TEM images of Fe<sub>3</sub>O<sub>4</sub>@SiO<sub>2</sub>-TCT/B<sub>5</sub>-Cu(II) (a and b).



Elt	Line	Int	W%	A%
C	Ka	29.8	7.89	13.06
N	Ka	19.8	4.27	6.06
O	Ka	852.0	49.77	61.85
Si	Ka	1514.3	16.38	11.59
Fe	Ka	461.4	15.27	5.43
Cu	Ka	102.6	6.42	2.01
			100.00	100.00

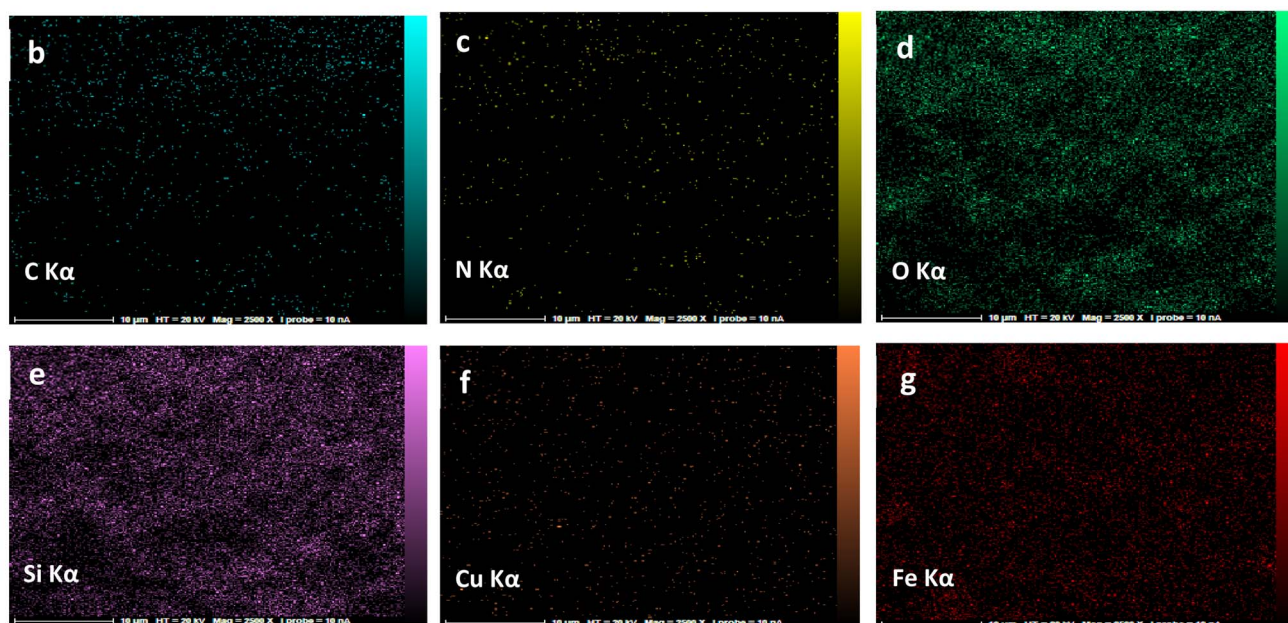


Fig. 4 EDAX analysis of Fe<sub>3</sub>O<sub>4</sub>@SiO<sub>2</sub>-TCT/B<sub>5</sub>-Cu(II) (a) and element-mapping images of Fe<sub>3</sub>O<sub>4</sub>@SiO<sub>2</sub>-TCT/B<sub>5</sub>-Cu(II) (b-g).



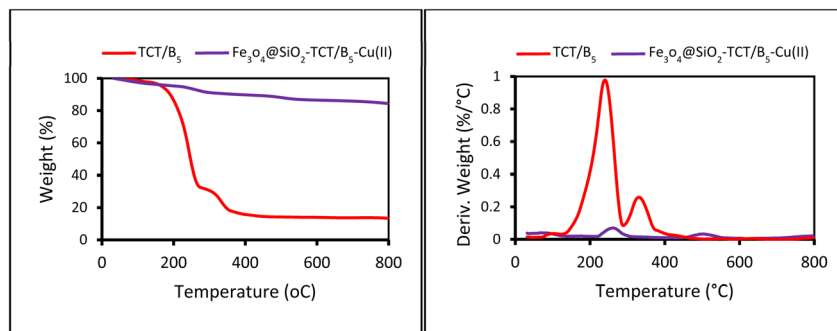
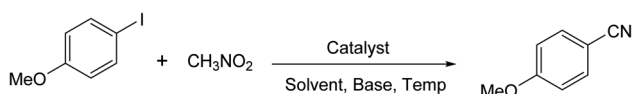


Fig. 6 TGA-DTG of TCT/B<sub>5</sub> (red curve) and Fe<sub>3</sub>O<sub>4</sub>@SiO<sub>2</sub>-TCT/B<sub>5</sub>-Cu(II) (violet curve).



Scheme 2 The model reaction for cyanation of aryl halides.

can be shown, TCT/B<sub>5</sub> nanoparticles are porous and irregular in shape. The TCT/B<sub>5</sub> nanoparticles have mean diameter of 36 nm. The morphology of the prepared Fe<sub>3</sub>O<sub>4</sub>@SiO<sub>2</sub>-TCT/B<sub>5</sub>-Cu(II) nanoparticles is a combination of the spherical Fe<sub>3</sub>O<sub>4</sub>@SiO<sub>2</sub> nanoparticles with the porous and irregular structure of the TCT/B<sub>5</sub> ligand with mean diameter of 38 nm, which is well showed in Fig. 3c and d.

**3.2.4. EDAX.** EDAX analysis confirmed that the final catalyst contains the expected elements of C, O, N, Fe, Si, and Cu with wt% of 7.89, 49.77, 4.27, 15.27, 16.38 and 6.42, respectively. Additionally, from EDAX element mapping images (Fig. 4b-h)

can be also concluded that TCT/B<sub>5</sub> and Cu(II) have a uniform distribution on the surface of Fe<sub>3</sub>O<sub>4</sub>@SiO<sub>2</sub>.

**3.2.5. TEM.** The TEM images of Fe<sub>3</sub>O<sub>4</sub>@SiO<sub>2</sub>-TCT/B<sub>5</sub>-Cu(II) have been presented in Fig. 5. There are two different morphologies in TEM images of Fe<sub>3</sub>O<sub>4</sub>@SiO<sub>2</sub>-TCT/B<sub>5</sub>-Cu(II), which can be attributed to the ligand and Fe<sub>3</sub>O<sub>4</sub> or Cu(II) NPs. The magnetic core can be seen as a dark spot inside the bright, spherical Cu(II) triazine-based complex, according to the observation from the TEM images.

**3.2.6. TGA.** The thermal degradation and thermal stability of TCT/B<sub>5</sub> and Fe<sub>3</sub>O<sub>4</sub>@SiO<sub>2</sub>-TCT/B<sub>5</sub>-Cu(II) nanoparticles were estimated by TGA-DTG analysis. The TGA of TCT/B<sub>5</sub> (Fig. 6) showed two main weight losses in the range of 150–800 °C. When the temperature increased from 150 to 300 °C, the pyrolysis of TCT/B<sub>5</sub> particles occurred with a mass loss of about 65%, which can be assigned to the degradation of main chains and aromatic rings. The second weight loss of about 15% between 300–450 °C can be related to the oxidation of carbon.

Table 1 Optimization conditions for Fe<sub>3</sub>O<sub>4</sub>@SiO<sub>2</sub>-TCT/B<sub>5</sub>-Cu(II)-catalyzed cyanation reaction<sup>a</sup>

Entry	Catalyst	Catalyst (mg)	Base	Solvent	Temp. (°C)	Yield <sup>b</sup> (%)
1	—	—	K <sub>2</sub> CO <sub>3</sub>	DMSO	100	0
2	Cu(OAc) <sub>2</sub>	10 mol%	K <sub>2</sub> CO <sub>3</sub>	DMSO	100	38
3	Fe <sub>3</sub> O <sub>4</sub> @SiO <sub>2</sub> -TCT/B <sub>5</sub>	30	K <sub>2</sub> CO <sub>3</sub>	DMSO	100	0
4	Fe <sub>3</sub> O <sub>4</sub> @SiO <sub>2</sub> -TCT/B <sub>5</sub> -Cu(II)	30	K <sub>2</sub> CO <sub>3</sub>	DMSO	100	94
5	Fe <sub>3</sub> O <sub>4</sub> @SiO <sub>2</sub> -TCT/B <sub>5</sub> -Cu(II)	30	K <sub>2</sub> CO <sub>3</sub>	K <sub>2</sub> CO <sub>3</sub> /glycerol (1 : 5)	100	10
6	Fe <sub>3</sub> O <sub>4</sub> @SiO <sub>2</sub> -TCT/B <sub>5</sub> -Cu(II)	30	K <sub>2</sub> CO <sub>3</sub>	CH <sub>3</sub> OH	100	70
7	Fe <sub>3</sub> O <sub>4</sub> @SiO <sub>2</sub> -TCT/B <sub>5</sub> -Cu(II)	30	K <sub>2</sub> CO <sub>3</sub>	Toluene	100	65
8	Fe <sub>3</sub> O <sub>4</sub> @SiO <sub>2</sub> -TCT/B <sub>5</sub> -Cu(II)	30	K <sub>2</sub> CO <sub>3</sub>	DMF	100	85
9	Fe <sub>3</sub> O <sub>4</sub> @SiO <sub>2</sub> -TCT/B <sub>5</sub> -Cu(II)	30	K <sub>2</sub> CO <sub>3</sub>	CH <sub>3</sub> CN	100	76
10	Fe <sub>3</sub> O <sub>4</sub> @SiO <sub>2</sub> -TCT/B <sub>5</sub> -Cu(II)	30	NaHCO <sub>3</sub>	DMSO	100	51
11	Fe <sub>3</sub> O <sub>4</sub> @SiO <sub>2</sub> -TCT/B <sub>5</sub> -Cu(II)	30	NaOH	DMSO	100	82
12	Fe <sub>3</sub> O <sub>4</sub> @SiO <sub>2</sub> -TCT/B <sub>5</sub> -Cu(II)	30	(CH <sub>3</sub> ) <sub>2</sub> NH	DMSO	100	59
13	Fe <sub>3</sub> O <sub>4</sub> @SiO <sub>2</sub> -TCT/B <sub>5</sub> -Cu(II)	30	DABCO	DMSO	100	68
14	Fe <sub>3</sub> O <sub>4</sub> @SiO <sub>2</sub> -TCT/B <sub>5</sub> -Cu(II)	20	K <sub>2</sub> CO <sub>3</sub>	DMSO	100	84
15	Fe <sub>3</sub> O <sub>4</sub> @SiO <sub>2</sub> -TCT/B <sub>5</sub> -Cu(II)	10	K <sub>2</sub> CO <sub>3</sub>	DMSO	100	71
16	Fe <sub>3</sub> O <sub>4</sub> @SiO <sub>2</sub> -TCT/B <sub>5</sub> -Cu(II)	40	K <sub>2</sub> CO <sub>3</sub>	DMSO	100	94
17	Fe <sub>3</sub> O <sub>4</sub> @SiO <sub>2</sub> -TCT/B <sub>5</sub> -Cu(II)	30	K <sub>2</sub> CO <sub>3</sub>	DMSO	110	94
18	Fe <sub>3</sub> O <sub>4</sub> @SiO <sub>2</sub> -TCT/B <sub>5</sub> -Cu(II)	30	K <sub>2</sub> CO <sub>3</sub>	DMSO	90	81
19	Fe <sub>3</sub> O <sub>4</sub> @SiO <sub>2</sub> -TCT/B <sub>5</sub> -Cu(II)	30	K <sub>2</sub> CO <sub>3</sub>	DMSO	100	95 <sup>c</sup>
20	Fe <sub>3</sub> O <sub>4</sub> /Cu(II)	30	K <sub>2</sub> CO <sub>3</sub>	DMSO	100	33
21	Fe <sub>3</sub> O <sub>4</sub> @SiO <sub>2</sub> -Cu(II)	30	K <sub>2</sub> CO <sub>3</sub>	DMSO	100	39

<sup>a</sup> Reaction conditions: 4-iodoanisole (1 mmol or 0.234 g), nitromethane (3 mmol or 0.183 g), base (1 mmol), and catalyst (30 mg, 0.3 mol%), 12 h, 100 °C. <sup>b</sup> Isolated yield. <sup>c</sup> K<sub>2</sub>CO<sub>3</sub> (2 mmol).



**Table 2** Synthesis of benzonitrile derivatives by  $\text{Fe}_3\text{O}_4@\text{SiO}_2\text{-TCT/B}_5\text{-Cu(II)}$

Entry	Substrate	Product	Yield <sup>b</sup> (%)
		<b>2(a-i)</b>	
1			X = I, 61 X = Br, 45
2			X = I, 80 X = Br, 73
3			67
4			63
5			X = I, 86 X = Br, 78
6			87
7			43
8			X = I, 78 X = Br, 70

**Table 2** (Contd.)

Entry	Substrate	Product	Yield <sup>b</sup> (%)
		<b>2(a-i)</b>	
9			X = I, 94 X = Br, 88

<sup>a</sup> Reaction conditions: 4-iodoanisole (1 mmol or 0.234 g), nitromethane (3 mmol or 0.183 g), potassium carbonate (1 mmol or 0.138 g), and the catalyst (30 mg), 12 h, 100 °C. <sup>b</sup> Isolated yield.

As shown in the TGA-DTG of  $\text{Fe}_3\text{O}_4@\text{SiO}_2\text{-TCT/B}_5\text{-Cu(II)}$ , the prepared nanoparticles showed higher stability than TCT/B<sub>5</sub>. The first main weight loss of  $\text{Fe}_3\text{O}_4@\text{SiO}_2\text{-TCT/B}_5\text{-Cu(II)}$  (about 6%) was observed in the range of 220–340 °C, indicating the degradation of organic contents. The second one (mass loss of 5%) was observed in the range of 460–550 °C, which can be attributed to the decomposition of the remaining organic moieties and oxidation of carbon.

### 3.3. Application of $\text{Fe}_3\text{O}_4@\text{SiO}_2\text{-TCT/B}_5\text{-Cu(II)}$ catalyst in cyanation reaction

After characterization of the  $\text{Fe}_3\text{O}_4@\text{SiO}_2\text{-TCT/B}_5\text{-Cu(II)}$  catalyst, we studied its catalytic performance in the cyanation reaction of aryl halides using  $\text{CH}_3\text{NO}_2$  as the cyanide resource (Scheme 2). In order to optimize the reaction conditions, we selected the cyanation of 4-iodoanisole with  $\text{CH}_3\text{NO}_2$  as the model reaction (Table 1). First, the cyanation reaction was evaluated in the absence of a catalyst (entry 1), no product was obtained under this condition, confirming the need for a catalyst to afford the desired product. The reaction was also tested in the presence of  $\text{Fe}_3\text{O}_4@\text{SiO}_2\text{-TCT/B}_5$  as a catalyst and no product was detected, indicating the necessity of copper for the formation an ideal product. The impacts of solvent, base, temperature, and amount of catalyst were studied to improve the reaction yield. To investigate the role of solvent in the cyanation reaction, a variety of solvents were applied in the reaction (entries 4–9). DMSO was chosen as the best solvent. Comparison between different bases used (entries 10–13), exhibited that  $\text{K}_2\text{CO}_3$  has the best efficiency to form the cyanated product. Based on the catalyst loading study, various amounts of catalyst were tested in this reaction. The amount of 30 mg was found to be the best value of catalyst for high conversion under the reaction conditions. The model reaction in presence of lower values of the catalyst resulted in a decrease



Table 3 Comparison of the current approach with previous reported methods for benzonitrile synthesis

Entry	Catalyst	Condition	Yield <sup>a</sup> (%)	Recyclability (run)	Reference
1	$\gamma$ -Fe <sub>2</sub> O <sub>3</sub> -Pd-NHC- <i>n</i> -butyl-SO <sub>3</sub> Na	Aryl halide (1 mmol), K <sub>4</sub> [Fe(CN) <sub>6</sub> ]·3H <sub>2</sub> O (1.2 mmol), Et <sub>3</sub> N (4 mmol), H <sub>2</sub> O (6 mL), catalyst (0.2 mol%)	94	6	31
2	CuI/Pd(II)-AOFs	Aryl halide (10.0 mmol), potassium ferrocyanide (4.0 mmol), Cu(I)Pd(II)-AOFs (6 mol%), Na <sub>2</sub> CO <sub>3</sub> (10.0 mmol), DMAC, reflux	98	4	32
3	Fe <sub>3</sub> O <sub>4</sub> @PMDP/Pd	Aryl halide (1.0 mmol), K <sub>4</sub> [Fe(CN) <sub>6</sub> ] (0.17 mmol), Fe <sub>3</sub> O <sub>4</sub> @PMDP/Pd (1.5 mol%), Na <sub>2</sub> CO <sub>3</sub> (1.5 mmol), DMF(3 mL), 120 °C	95	8	33
4	Pd NPs@β-CD	Aryl halide (1.5 mmol), potassium ferrocyanide (0.2 mmol), Na <sub>2</sub> CO <sub>3</sub> (1.8 mmol), catalyst (0.05 mol%), DMF, 120 °C	95	8	34
5	Ni(acac) <sub>2</sub> (5 mol%), AlCl <sub>3</sub> (10 mol%), bpy (30 mol%)	Aryl halide (0.2 mmol), Ni(acac) <sub>2</sub> (5 mol%), AlCl <sub>3</sub> (10 mol%), Bpy (30 mol%), ZnO(1.0 equiv.), HCONH <sub>2</sub> (1.0 mL), 1,2-DME (1.5 mL), 145 °C	90	—	35
6	CuF <sub>2</sub>	Aryl halide (0.2 mmol), CO(NH <sub>2</sub> ) <sub>2</sub> (4 equiv.), CuF <sub>2</sub> (20 mol%), Li <sub>2</sub> CO <sub>3</sub> (3 equiv.), O <sub>2</sub> , DMSO, 150 °C	87	—	36
7	Fe <sub>3</sub> O <sub>4</sub> @SiO <sub>2</sub> -TCT/B <sub>5</sub> -Cu(II)	Aryl halide (1 mmol), CH <sub>3</sub> NO <sub>2</sub> (3 mmol), K <sub>2</sub> CO <sub>3</sub> (1 mmol), catalyst (30 mg), 100 °C	100	5	This work

<sup>a</sup> Isolated yield.

in the yield of the cyanation product (entries 14 and 15). Decreasing the reaction temperature to 90 °C brought down the yield to 81% (entry 18). By increasing the temperature to 110 °C (entry 17), no change in the yield of the product was observed. The cyanation reaction was carried out in the presence of copper on substrates Fe<sub>3</sub>O<sub>4</sub> and Fe<sub>3</sub>O<sub>4</sub>@SiO<sub>2</sub>. These substrates

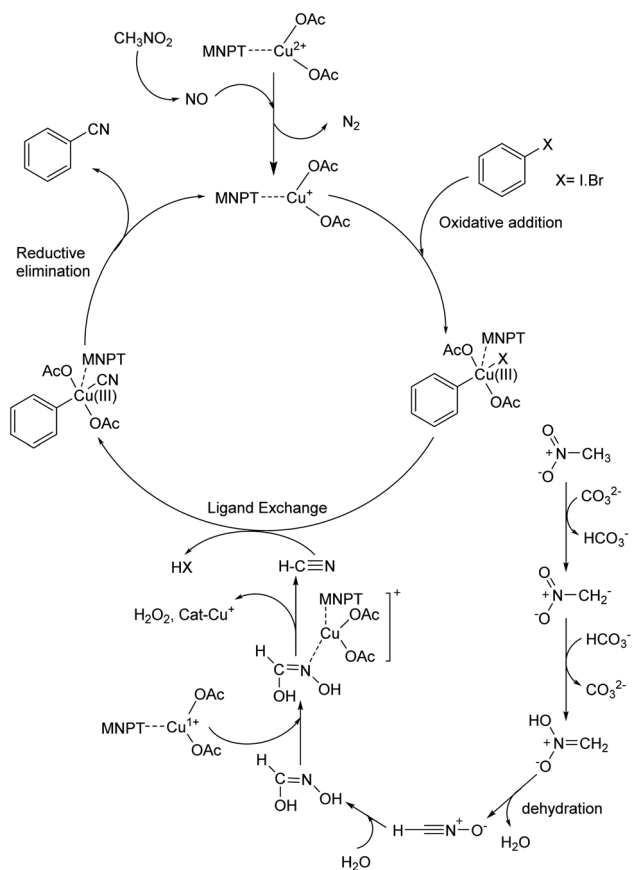
are free of vitamin B<sub>5</sub> to investigate the importance of the ligand in this reaction. According to the results, the importance of vitamin B<sub>5</sub> in the prepared composite is concluded. The presence of vitamin B<sub>5</sub> in the structure of catalyst is essential and enhances efficiency (entries 20 and 21).

In order to evaluate the role of substituent groups, various aryl halides bearing both electron-rich and electron-poor groups were tested in this reaction (Table 2). Under the optimum reaction conditions, aryl iodides and bromides containing various substituents smoothly underwent the cyanation reaction to generate the corresponding benzonitriles in good to excellent yields. Aryl iodides provided higher reaction efficiency than aryl bromides due to the weakness of the C-I bond compared to C-Br. As shown in Table 2, *O*-substituted aryl halides (**2f**, **2k** and **2l**) gave lower yields compared to *P*-substituents due to the hindrance effect.

The catalyst efficiency of Fe<sub>3</sub>O<sub>4</sub>@SiO<sub>2</sub>-TCT/B<sub>5</sub>-Cu(II) and effectiveness of the present approach were compared with the previous researches. As shown in Table 3, it benefits from the use of copper as an inexpensive and readily available transition metal along with a copper-based heterogeneous catalyst, which can be easily separated from the reaction mixture. As an important and considerable advantage of this approach, it can be mentioned the use of nitromethane as an inexpensive, available, non-metallic CN source with low toxicity, which is highly efficient for producing desirable products in the presence of the Fe<sub>3</sub>O<sub>4</sub>@SiO<sub>2</sub>-TCT/B<sub>5</sub>-Cu(II) catalyst.

### 3.4. Mechanism

A possible mechanism for this reaction is proposed based on a similar previous report.<sup>19a,37,38</sup> Thermochemical studies show that CH<sub>3</sub>NO<sub>2</sub> can be decomposed into CO and NO at high temperatures. The released NO in the reaction medium interacts with Cu(II) in the catalyst and reduces Cu(II) to Cu(I). The 16-electron Cu(I) complex undergoes an oxidative addition reaction with aryl halide to form complex A. The 18-electron A complex performs ligand exchange in presence of HCN (generated from



Scheme 3 Plausible mechanism of cyanation reaction.



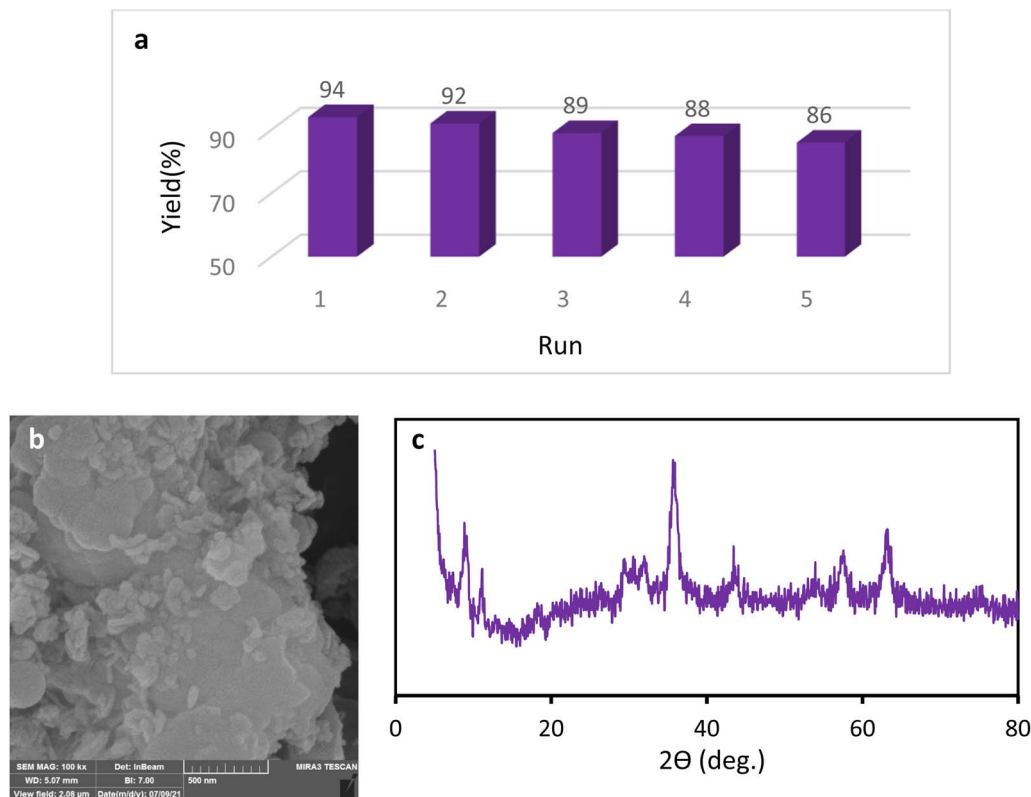


Fig. 7 Recycling of the  $\text{Fe}_3\text{O}_4@\text{SiO}_2\text{-TCT/B}_5\text{-Cu(II)}$  nanocatalyst (a), SEM image (b) and XRD pattern (c) of the recovered  $\text{Fe}_3\text{O}_4@\text{SiO}_2\text{-TCT/B}_5\text{-Cu(II)}$  nanocatalyst.

$\text{CH}_3\text{NO}_2$  using base) and produces B complex. Finally, complex B after a reductive elimination affords the cyanation product and the catalyst returns to the catalytic cycle (Scheme 3).

### 3.5. Catalyst recyclability

We examined the recyclability and reusability of our catalyst in the cyanation reaction of 4-ome-iodobenzene in presence of  $\text{CH}_3\text{NO}_2$  under the optimized conditions. The recyclability of the catalyst was evaluated for 5 consecutive runs. After each run of the reaction, catalyst was isolated by an external magnet, washed with EtOH and applied for the next run. As shown in Fig. 7, the catalytic activity has not changed significantly after 5 runs. The recycled catalyst in the 5th run was studied with SEM, XRD, and ICP analyses to investigate the catalyst stability under reaction conditions. The XRD pattern and SEM image have exhibited no significant difference with fresh catalyst. ICP analysis provided the Cu content of the recovered nanocatalyst after 5th run ( $0.65 \text{ mmol g}^{-1}$ ) which did not show a significant decrease compared to that of the original catalyst.

## 4 Conclusion

In conclusion, a novel and efficient catalytic approach for the synthesis of aryl nitriles in presence of  $\text{Fe}_3\text{O}_4@\text{SiO}_2\text{-TCT/B}_5\text{-Cu(II)}$  nanocatalyst and nitromethane as a non-toxic, inexpensive and readily available cyanating source has been developed. The aryl nitriles were obtained in moderate to good yields. The

prepared heterogeneous nanocatalyst can be readily separated from the reaction mixture by magnetic filtration and recovered for at least five cycles without a significant loss of its activity.

## Ethical statement

This research does not involve human participants and/or animals.

## Data availability

The data that supports the findings of this study are available in the ESI† of this article.

## Author contributions

Conceptualization: Farzaneh Karimi, Masoumeh Jadidi Nejad; methodology: Farzaneh Karimi, Masoumeh Jadidi Nejad; formal analysis and investigation: Farzaneh Karimi and Masoumeh Jadidi Nejad; writing-original draft preparation: Masoumeh Jadidi Nejad, Arefe Salamatmanesh; writing-review and editing: Arefe Salamatmanesh, Masoumeh Jadidi Nejad; funding acquisition: Akbar Heydari; resources: Akbar Heydari; supervision: Akbar Heydari.



## Conflicts of interest

There are no conflicts of interest to declare.

## Acknowledgements

We are grateful to Tarbiat Modares University for financial support of this work.

## References

- (a) J. Magano and J. R. Dunetz, *Chem. Rev.*, 2011, **111**, 2177–2250; (b) B. Patel, C. R. Firkin, E. W. Snape, S. L. Jenkin, D. Brown, J. G. K. Chaffey, P. A. Hopes, C. D. Reens, M. Butters and J. D. Moseley, *Org. Process Res. Dev.*, 2012, **16**, 447–460; (c) A. Zanka, M. Nishiwaki, Y. Morinaga and T. Inoue, *Org. Process Res. Dev.*, 1998, **2**, 230–237.
- (a) O. Kivrakidou, S. Bräse, F. Hülshorst and N. Griebenow, *Org. Lett.*, 2004, **6**, 1143–1146; (b) R. C. Larock, *Comprehensive organic transformations*, Wiley Online Library, 1989.
- T. Sandmeyer, *Ber. Dtsch. Chem. Ges.*, 1884, **17**, 2650–2653.
- (a) J. Von Braun and G. Manz, *Justus. Liebigs Ann. Chem*, 1931, **488**, 111–126; (b) K. W. Rosenmund and E. Struck, *Ber. Dtsch. Chem. Ges.*, 1919, **52**, 1749–1756.
- C. Yang and J. M. Williams, *Org. Lett.*, 2004, **6**, 2837–2840.
- B. A. Anderson, E. C. Bell, F. O. Ginah, N. K. Harn, L. M. Pagh and J. P. Wepsiec, *J. Org. Chem.*, 1998, **63**, 8224–8228.
- F. Jin and P. N. Confalone, *Tetrahedron Lett.*, 2000, **41**, 3271–3273.
- H.-Q. Do and O. Daugulis, *Org. Lett.*, 2010, **12**, 2517–2519.
- X. Chen, X.-S. Hao, C. E. Goodhue and J.-Q. Yu, *J. Am. Chem. Soc.*, 2006, **128**, 6790–6791.
- Z. Jiang, Q. Huang, S. Chen, L. Long and X. Zhou, *Adv. Synth. Catal.*, 2012, **354**, 589–592.
- C. Qi, X. Hu and H. Jiang, *Chem. Commun.*, 2017, **53**, 7994–7997.
- Y. Zhu, M. Zhao, W. Lu, L. Li and Z. Shen, *Org. Lett.*, 2015, **17**, 2602–2605.
- Q. Wen, J. Jin, B. Hu, P. Lu and Y. Wang, *RSC Adv.*, 2012, **2**, 6167–6169.
- H. Xu, P.-T. Liu, Y.-H. Li and F.-S. Han, *Org. Lett.*, 2013, **15**, 3354–3357.
- J. Kim, H. Kim and S. Chang, *Org. Lett.*, 2012, **14**, 3924–3927.
- X. Ren, J. Chen, F. Chen and J. Cheng, *Chem. Commun.*, 2011, **47**, 6725–6727.
- A. B. Pawar and S. Chang, *Chem. Commun.*, 2014, **50**, 448–450.
- S. Xu, X. Huang, X. Hong and B. Xu, *Org. Lett.*, 2012, **14**, 4614–4617.
- (a) R. Saikia, S. Dey Baruah, R. C. Dekka, A. J. Thakur and U. Bora, *Eur. J. Org. Chem.*, 2019, 6211–6216; (b) Y. Ogiwara, H. Morishita, M. Sasaki, H. Imai and N. Sakai, *Chem. Lett.*, 2017, **46**, 1736–1739.
- M. Sundermeier, A. Zapf, S. Mutyala, W. Baumann, J. Sans, S. Weiss and M. Beller, *Chem.–Eur. J.*, 2003, **9**, 1828–1836.
- D.-G. Yu, T. Gensch, F. de Azambuja, S. Vásquez-Céspedes and F. Glorius, *J. Am. Chem. Soc.*, 2014, **136**, 17722–17725.
- X. Zhang, A. Xia, H. Chen and Y. Liu, *Org. Lett.*, 2017, **19**, 2118–2121.
- A. B. Khemnar, D. N. Sawant and B. M. Bhanage, *Tetrahedron Lett.*, 2013, **54**, 2682–2684.
- L. Zhao, Y. Dong, Q. Xia, J. Bai and Y. Li, *J. Org. Chem.*, 2020, **85**, 6471–6477.
- (a) M. Nasrollahzadeh, S. M. Sajadi, A. Rostami-Vartooni and M. Khalaj, *J. Colloid Interface Sci.*, 2015, **453**, 237–243; (b) A. Modak, J. Mondal and A. Bhaumik, *Green Chem.*, 2012, **14**, 2840–2855; (c) H. Yu, R. N. Richey, W. D. Miller, J. Xu and S. A. May, *J. Org. Chem.*, 2011, **76**, 665–668; (d) M. Çalışkan and T. Baran, *Int. J. Biol. Macromol.*, 2021, **174**, 120–133.
- (a) H. Veisi, T. Tamoradi, A. Rashtiani, S. Hemmati and B. Karmakar, *J. Ind. Eng. Chem.*, 2020, **90**, 379–388; (b) T. Baran, *Carbohydr. Polym.*, 2020, **237**, 116105; (c) M. Jadidi Nejad and A. Heydari, *Appl. Organomet. Chem.*, 2021, **35**, e6368; (d) A. Salamatmanesh and A. Heydari, *Appl. Catal., A*, 2021, **624**, 118306.
- H. Jiang, J. Jiang, H. Wei and C. Cai, *Catal. Lett.*, 2013, **143**, 1195–1199.
- Y. Cai, H. Yuan, Q. Gao, L. Wu, L. Xue, N. Feng and Y. Sun, *Catal. Lett.*, 2022, 1–17.
- B. Tamami, M. Mohaghegh Nezhad, S. Ghasemi and F. Farjadian, *Phosphorus, Sulfur Silicon Relat. Elem.*, 2016, **191**, 123–128.
- Y. Ogiwara, H. Morishita, M. Sasaki, H. Imai and N. Sakai, *Chem. Lett.*, 2017, **46**, 1736–1739.
- F. O. Chahkamali, S. Sobhani and J. M. Sansano, *Catal. Lett.*, 2021, 1–19.
- Z.-C. Wu, Q. Yang, X. Ge, Y.-M. Ren, R.-C. Yang and T.-X. Tao, *Catal. Lett.*, 2017, **147**, 1333–1338.
- H. Veisi, S. Hemmati and P. Safarimehr, *J. Catal.*, 2018, **365**, 204–212.
- T. Baran and M. Nasrollahzadeh, *Inorg. Chem. Commun.*, 2020, **119**, 108117.
- L. Yang, Y.-T. Liu, Y. Park, S.-W. Park and S. Chang, *ACS Catal.*, 2019, **9**, 3360–3365.
- K. Zheng, B. Liu, S. Chen and F. Chen, *Tetrahedron Lett.*, 2013, **54**, 5250–5252.
- X. Li, X. Ren, H. Wu, W. Zhao, X. Tang and G. Huang, *Chin. Chem. Lett.*, 2021, **32**, 9–12.
- M.-H. Shen, T.-B. Wan, X.-R. Huang, Y. Li, D.-H. Qian, H.-D. Xu and D. Xu, *Chin. Chem. Lett.*, 2021, **32**, 2297–2300.

